

This is the accepted manuscript made available via CHORUS. The article has been published as:

## Collapse of elongated voids in porous energetic materials: Effects of void orientation and aspect ratio on initiation

Nirmal Kumar Rai, Martin J. Schmidt, and H. S. Udaykumar

Phys. Rev. Fluids **2**, 043201 — Published 28 April 2017

DOI: [10.1103/PhysRevFluids.2.043201](https://doi.org/10.1103/PhysRevFluids.2.043201)

# **Collapse of Elongated Voids in porous Energetic Materials: Effects of void orientation and aspect ratio on initiation**

Nirmal Kumar Rai<sup>1</sup>, Martin J Schmidt<sup>2</sup> and H. S. Udaykumar<sup>1,\*</sup>

<sup>1</sup>Department of Mechanical and Industrial Engineering, The University of Iowa, Iowa City, IA-52242, USA

<sup>2</sup>AFRL-RW, Eglin Air Force Base, Florida 32542, USA

## **ABSTRACT**

Sensitivity of porous energetic materials depends on meso-structural heterogeneities such as voids, defects, cracks and grain boundaries. Meso-structure of pressed explosives contains voids of arbitrary shapes including elongated voids of various orientations and aspect ratios. Meso-scale simulations to date have analyzed the effect of void morphology on the sensitivity of energetic materials for idealized shapes such as cylindrical, conical, elliptical etc. This work analyzes the sensitivity behavior of elongated voids in a HMX matrix subject to shock loading. Simulations show that sensitivity of elongated voids depends strongly on orientation as well as aspect ratio. Ranges of orientations and aspects ratios are identified that enhance or inhibit initiation. Insights obtained from single elongated void analyses are used to identify sensitive locations in an imaged meso-structure of a pressed explosive sample.

*Keywords: Pressed Energetic Materials, Hot Spot, Ignition Sensitivity, HMX, Elongated Voids, Void orientation*

## **I. INTRODUCTION**

Heterogeneous energetic materials find applications in many engineering systems such as propulsive devices, munitions and actuators. They are formulated by blending energetic crystals with plastic binders or physically pressing energetic crystals to form pressed pellets. Pressed energetic materials [1] are generally highly sensitive. However, their sensitivity can vary based on the meso-structural morphology in the formed pellet. The meso-structure of pressed explosives consists of energetic crystals and voids (in the form of crystal boundaries, defects etc). It is well established that the interaction of a shock wave with these meso-structural heterogeneities can lead to the formation of hot spots [2,3]. Chemical reactions and heat release initiate at such hot spot locations and grow into the surrounding material. There are various mechanisms [3] through which hot spots can originate, such as void collapse, frictional heating between the energetic crystals, adiabatic shear banding etc. Among these mechanisms, void collapse is considered to be predominant in the shock initiation regime [4–7,8].

Meso-scale simulations have been used in the past [4–12] to understand the effect of meso-structural heterogeneities on the sensitivity behavior of energetic materials. Several groups have performed simulations of void collapse; voids have often been assumed to assume idealized shape such as cylindrical, spherical, conical etc. The effects of void shape have been examined to

a limited extent in previous work suggesting that some void morphologies can lead to stronger hot spots than others [5,8,11,12]. Most of the previously studied shapes were modest deviations from spherical or cylindrical void shapes. However, as seen in a real (imaged) meso-structure of a pressed explosive (Figure 1) voids are arbitrarily shaped and a large number of them can be elongated in shape. This work is an attempt to understand the sensitivity behavior of such elongated voids under shock loading. A further objective is to connect the collapse behavior and hot spot intensities of elongated voids with the initiation sensitivity of a real (i.e. imaged) porous explosive.

The phenomenon of void collapse has been extensively studied in the past via experimental studies [13–15] and numerical simulations [4–12], but the focus has been limited to the study of idealized shape voids such as cylindrical, elliptical, conical or spherical voids. There are no experimental works that consider the study of non-cylindrical voids such as shown in the real meso-structure of the pressed explosives (Figure 1). Also, there have been sparse attempts made to analyze the behavior of non-circular voids using meso-scale simulations [5,8,10–12]. In these works, limited attempts were made to study the effect of void morphology on the sensitivity of energetic materials using both inert and reactive meso-scale simulations. Notable early work includes Tran et al. [5] where inert calculations were performed on spherical and triangular/conical voids in HMX. It was observed that the spherical void produced a low strength hot spot as compared to the triangular void. Also, the triangular void with its apex pointed towards the shock wave generated a low strength hot spot as compared to a triangle with its base pointing towards the incident shock. Levesque and Vitello [8] also analyzed the effect of void morphology on the hot spot temperature for TATB using inert meso-scale simulations. Spherical, cylindrical, elliptical and conical/triangular voids were considered in their study. Size effects of each of these void geometries was also studied. It was shown that elliptical and cylindrical voids when arranged in line with their longest dimension (i.e. along the major axis for the elliptical void and along the length for the cylindrical void) produced much stronger hot spots than the spherical void for the same shock strength and volume fraction. Also, in agreement with Tran et al.'s [5] work, conical voids facing their apex towards the incident shock were found to be less sensitive when compared to the case where the base of the cone faced the incident shock. Levesque and Vitello [8] pointed out that void morphology has a significant effect on the hot spot temperature and that spherical voids must be recognized as idealized shapes when discussing sensitivity of porous energetic materials. Although the inert meso-scale simulations have been able to illustrate the effect of various void morphologies on the hot spot temperature, they cannot yield insights into whether sustained reactions can initiate from a given hot spot. This requires reactive meso-scale calculations.

Reactive meso-scale simulations have recently been employed to study the effect of void morphology on the sensitivity of energetic materials. Kapila et al. [11] performed reactive simulations on three different void shapes: spherical, prolate spheroid (long void) and oblate spheroid (tall void) in HMX. The effect of size of the above mentioned three void shapes was also studied. It was observed that small size voids are not sufficient for initiating reactions. Amongst the three void shapes, the oblate spheroid (tall void) was found to be most efficient in the generation of high strength that can lead to detonation. The recent work by Springer et al. [12] analyzed the effect of void morphology on the shock initiation and reaction rate in HMX.

Spherical, elliptical and conical voids were considered in the analysis. It was shown that elliptical and conical voids of high aspect ratio lead to increased sensitivity. Also, the effect of void morphology is shown to be dominant in the low shock pressure loading situations. It is clear from these meso-scale studies that void shape plays a crucial role in the sensitivity of porous energetic materials.

In past meso-scale efforts, although different shapes and size effects were analyzed, few studies directly correlated these effects to the behavior of a real meso-structure of an explosive. One of the first such attempts is a recent work [10] that analyzed the response to shock loading of imaged meso-structures and correlated the orientation of the elongated voids to initiation sensitivity. However, that study did not comprehensively cover the effect various aspects of void morphology on sensitivity. Also, the grid resolution used in the study [10] was perhaps inadequate to accurately capture all aspects of the dynamics of slender voids. In the real meso-structures, voids of arbitrary shape and sizes are present. Figure 1 shows the SEM image of two pressed explosive meso-structure classified as coarse-grained Class III explosives and fine-grained Class V explosives. It can be seen that the majority of the voids present in the meso-structure are of elongated shapes with various aspect ratios and orientations. In this work, using high resolution numerical simulations the effect of void morphology of elongated voids is investigated in detail; insights are obtained into the key geometrical features that influence sensitivity i.e. void orientation and aspect ratio.

The work presented in this paper is arranged as follows: section II presents a brief description of the governing equations, HMX material models, HMX reactive kinetics model and the numerical framework of a massively parallel Eulerian code SCIMITAR3D [16,17]; section III describes the computational set up used in the meso-scale analysis of the elongated voids; section IV presents the key results of the meso-scale analysis by examining the effect of orientation and aspect ratio of elongated voids. The understanding obtained from the numerical experiments of elongated voids is then used to explain the initiation behavior of an imaged Class III pressed energetic sample.

## II. FORMULATION

In the current Eulerian framework, the governing equations are comprised of a set of hyperbolic conservation laws [18] corresponding to the conservation of mass, momentum and energy:

$$\frac{\partial \rho}{\partial t} + \text{div}(\rho \vec{V}) = 0 \quad (1)$$

$$\frac{\partial \rho \vec{V}}{\partial t} + \text{div}(\rho \vec{V} \otimes \vec{V} - \sigma) = 0 \quad (2)$$



$$\frac{\partial \rho E}{\partial t} + \text{div}(\rho E \vec{V} - \sigma \vec{V}) = 0 \quad (3)$$

where,  $V$  is the velocity,  $\rho$  is density,  $E$  is the specific internal energy and  $\sigma$  is the Cauchy stress tensor. The stress state of material,  $\sigma$  can be decomposed into a deviatoric part,  $S$  and dilatational part,  $P$ :

$$\sigma = S - PI \quad (4)$$

The deviatoric stress  $S$  is obtained from the evolution equation in the rate form, by first updating the elastic response:

$$\frac{\partial \rho S}{\partial t} + \text{div}(\rho \vec{V} S) + \frac{2}{3} \rho G \text{tr}(D) I - 2 \rho G D = 0 \quad (5)$$

where,  $D$  is strain rate tensor, and  $G$  is the shear modulus of material. This step is followed by a radial return to the yield surface to account for plasticity. Further details on the elasto-plastic treatment can be found in previous papers [16,17].

In the current work, the energetic material considered is HMX. The constitutive and reactive models of HMX using in the current framework is discussed in a companion paper [19]. The governing equations of mass (Eq. (1)), momentum (Eq. (2)), energy (Eq. (3)) along with the evolution of deviatoric stresses are spatially discretized using a 3<sup>rd</sup>-order essentially non-oscillatory scheme [20] and numerically integrated using 3<sup>rd</sup>-order Runge-Kutta time stepping. The interfaces in the current framework are handled using the narrow-band level set approach [21]. The level set approach allows for tracking of the interfaces in a sharp manner and can handle large deformation of the materials as in the formation of material jets and collapse. Interfacial conditions are applied at the sharp interface locations using a modified ghost fluid method [22]. The complete description of the numerical framework can be found in previous work [16,17].

### III. COMPUTATIONAL SETUP

The sensitivity behavior of elongated voids is studied using reactive meso-scale simulations. In the current work sensitivity is characterized as a function of the strength of the imposed shock. A single elongated void in an otherwise homogeneous HMX material is considered. Figure 2 shows an elongated void of thickness  $a = 0.5 \mu\text{m}$  and length  $b = 10 \mu\text{m}$  oriented at an angle  $\theta$  with respect to the incident shock embedded in a uniform HMX matrix of size  $13 \mu\text{m} \times 10 \mu\text{m}$ . A shock load of prescribed strength and  $0.5 \text{ ns}$  pulse duration is applied at the west face of the domain boundary. The other domain boundaries including the east, north and south faces are modeled with outlet conditions.

The geometrical aspects of elongated voids such as orientation with respect to the incident shock and aspect ratio are varied to understand how these features can effect sensitivity. The numerical set up shown in Figure 2 remains the same for all the studies herein.

## IV. RESULTS

Extensive verification and validation of the current numerical framework for voids of circular cross section are presented in a companion paper [19]. In that paper the material models for HMX, the reactive kinetics models and the temperatures reached after void collapse have been carefully benchmarked against available numerical and experimental results. In this work the effect of orientation and aspect ratio on sensitivity of elongated voids is analyzed.

### A. Grid convergence study for the elongated voids

Grid resolution plays a crucial role in the meso-scale simulations of porous energetic materials. In a companion paper [19], the effect of grid resolution on reaction initiation is studied for the situation involving cylindrical voids. It is shown that the use of coarse grids under-predicts the hot spot temperature and leads to incorrect prediction of sensitivity. It is also shown that the grid resolution requirement for a cylindrical void depends on the shock strength. The grid resolution requirement become more stringent with increasing shock strength. For a cylindrical void, 700 grid points across the void diameter was found to be the required resolution; at that level of refinement the uncertainty associated with the grid resolution on ignition prediction is sufficiently small. Apart from the shock strength, the grid resolution requirement can also be effected by the void morphology. The dependency of grid resolution on void morphology has not been studied in previous meso-scale work [4–8,10]. Without such a study it is not possible to assess whether a meso-scale simulation produces accurate predictions of sensitivity of a porous energetic material sample. In particular, as shown in Figure 1 pressed explosives contain a distribution of elongated voids of various orientations and aspect ratios. Therefore, this section focuses on establishing the grid resolution required to obtain a converged solution for the void collapse of an elongated void.

The computational setup for the grid refinement study is shown in Figure 2, with an elongated void oriented at an angle of  $\theta = 45^\circ$  with respect to the incident shock. This first analysis is performed assuming HMX as an inert material i.e. switching off the reaction calculation. In the companion work [19] involving cylindrical voids it is observed that the grid resolution requirement becomes increasingly stringent with the increase in the shock strength. Therefore, for the elongated void the grid refinement study is performed for a high shock strength (1000  $m/s$  particle velocity); lower shock strength cases will then demand smaller number of grid points. An imposed shock corresponding to a particle velocity of 1000  $m/s$  and pulse duration of 0.5  $ns$  is applied at the west face of the domain boundary (Figure 2). Six different grid sizes corresponding to 10, 20, 30, 40, 60 and 80 grid points across the thickness ( $a = 0.5 \mu m$ ) of the elongated void are tested. The time variation of the maximum temperature in the domain is used as a measure through which grid convergence is established. Figure 3 shows the time variation of the maximum temperature for all the mentioned six grid sizes. It can be seen that with the use of finer grids, the collapse temperature increases. The use of coarse grids i.e. 10 – 20 grid points across the void thickness significantly under-predicts the collapse temperature. With sufficiently fine grid sizes i.e. 30 – 40 grid points across the void thickness the collapse temperature starts to converge and eventually saturates for grid corresponding to

60 points across the void thickness. Therefore, in the rest of this paper 40 points across the void thickness are used to resolve the elongated voids.

## **B. Effect of void morphology on the sensitivity behavior of energetic materials**

Voids of circular and triangular cross-sections have been used in the past to understand the behavior of porous energetic materials [4,6,7]. However, real meso-structure of explosives contain elongated or other irregular shaped voids which may impact on the sensitivity of the porous material. The effect of elongated void shapes is studied by comparing the ignition threshold of a cylindrical void and an elongated void of the same effective void area using reactive meso-scale simulations.

There are multiple ways through which reaction initiation can be identified in a reactive meso-scale simulation. For example, the initiation of chemical reaction and ignition in HMX can be indicated by the rise in temperature due to the initiation of exothermic reactions. Ignition can also be tracked via the rise in the total specific internal energy of the meso-scale sample. The total specific internal energy is calculated as:

$$e_T = \frac{\int_V \rho e dV}{\int_V \rho dV} \quad (6)$$

where,  $e_T$  is the total specific internal energy in the sample,  $\rho$  is the density and  $e$  is the computed specific internal energy field. The total internal energy is a scalar quantity that tracks the conversion of mechanical energy to heat through plastic dissipation, material jetting, impact and void collapse.

The reaction initiation and ignition in the material can also be indicated by the mass fraction of the final gaseous species. The volume average of the final gaseous species can be expressed as,

$$F = \frac{\int_V \rho Y_4 dV}{\int_V \rho dV} \quad (7)$$

where,  $F$  is the volume average of the final gaseous species,  $\rho$  is the density,  $Y_4$  is the mass fraction of the gaseous species,  $V$  is the volume.

The volume average of the final gaseous species over the domain indicates whether the reaction is initiated, is partially completed or fully completed. Therefore, the volume average of final gaseous species and total specific internal energy are used in this work to track reaction initiation and ignition.

### ***1. Ignition threshold for an elongated void***

The computational set up shown in Figure 2 is used to obtain the ignition threshold of elongated voids. The void is oriented at an angle of  $\theta = 45^\circ$  with respect to the incident shock. The shock pulse duration is kept constant at 0.5 ns for the study. Four different shock strengths, corresponding to 350, 500, 650 and 850 m/s particle velocity are considered.

The time variation of total specific internal energy is analyzed. Figure 4(a) shows the rise in the specific internal energy as the collapse of the void leads to the formation of a hot spot for

all of the shock speeds. However two distinct situations can arise *after* hot spot formation. Depending on the temperature and the size of the hot spot formed after the collapse, reaction can initiate or the hot spot can be extinguished. For the shock strengths of 350  $m/s$  and 500  $m/s$ , the hot spot formed is not intense enough and diffusion redistributes the hot spot energy to the surroundings leading to quenching of the hot spot. This is evident from Figure 4(a) which shows that after the formation of the hot spot the total specific internal remains a constant. For shock strengths of 650  $m/s$  and 850  $m/s$ , the hot spot formation is followed by reaction initiation and ignition in the material, which is indicated by the sharp rise of the total specific internal energy in Figure 4(a).

As the shock strength increases, the strength of the hot spot formed also increases and it takes less time to initiate reaction for a high strength hot spot. This can be observed in Figure 4(a) where the sharp rise in the total specific internal energy starts later for 650  $m/s$  shock and earlier for the 850  $m/s$  shock. The threshold for the elongated void (Figure 2) with thickness,  $a = 0.5 \mu m$  and length  $b = 10 \mu m$  oriented at an angle of  $\theta = 45^\circ$  with respect to the incident shock wave is observed to lie between 500  $m/s$  and 650  $m/s$ .

## ***2. Ignition threshold for a cylindrical void***

The effect of the void shape can be examined by comparing threshold of a cylindrical void of the same effective void area as the elongated void used in the previous case (Figure 2). The void area of the elongated void used in the previous analysis was  $5 \mu m^2$  which corresponds to a diameter of  $2.52 \mu m$  for the cylindrical void. Four different shock strengths with imposed particle speed of 500, 650, 850 and 1000  $m/s$  are used to identify the ignition threshold for the cylindrical void.

Figure 4(b) shows the time variation of the total specific internal energy. The 500, 650 and 850  $m/s$  cases do not lead to initiation. This can be seen in Figure 4(b) where the total specific internal energy settles to a constant value after the hot spot formation. For 1000  $m/s$  shock strength, the hot spot strength is sufficient to initiate chemical reaction and the reaction initiation can be seen in Figure 4(b) through a sharp rise in the total specific internal energy. The ignition threshold of the cylindrical void of  $2.52 \mu m$  is observed to lie between 850  $m/s$  and 1000  $m/s$  shock speed.

## ***3. Comparison of the sensitivity behavior of elongated and cylindrical void***

For the same void volume fraction of an elongated void oriented at an angle of  $\theta = 45^\circ$  and a cylindrical void, the ignition threshold for the elongated void lies between 500  $m/s$  and 650  $m/s$  and for cylindrical void it lies between 850  $m/s$  and 1000  $m/s$ . This indicates that elongated voids at certain orientations are more sensitive than cylindrical voids. It is useful to understand the cause of the heightened sensitivity of the elongated void relative to the cylindrical void. Figure 5 compares the collapse behavior of the two voids under the shock load of 650  $m/s$  and a pulse duration of 0.5  $ns$ . The collapse of the cylindrical void starts with the formation of a strong material jet at the upstream surface of the void (Figure 5(c)). The material jet impacts the downstream surface of the void leading to the formation of a primary blast wave and a local high temperature zone at the point of jet impact (Figure 5(c)). The initial jet impact also causes the

formation of two symmetrical lobes, i.e. secondary voids, which are formed from the initial cylindrical void (Figure 5(c)). These symmetrical lobes collapse under the combined influence of the initial shock load and the primary blast wave. The collapse of the symmetrical lobes causes further rise in the hot spot temperature (Figure 5(e)). In fact, this secondary collapse temperature can be significantly higher than the initial temperature rise caused by the jet impact (Figure 5(e)). The reaction may initiate either near the initial jet impact site or near the secondary collapse temperature depending on the strength of the shock. For the shock speed of  $650\text{ m/s}$ , the hot spot formed after both the primary and secondary collapse of the voids is unable to initiate reaction and the hot spot diffuses (Figure 5(g)). The collapse of an elongated void oriented at  $\theta = 45^\circ$  is different from the cylindrical void case as shown in Figure 5. The collapse of the elongated void involves successive pinching of the upstream surface of the void against the downstream surface (Figure 5(b) and Figure 5(d)), i.e. the jetting and impact mechanism does not operate in this case. Each pinching event causes the formation of a blast wave that strengthens with the continuing collapse along the length of the void (Figure 5(d)). With each pinching instance the strength of the resulting blast increases. This intensification subsequently pinches the void under increased shock loads and causes the formation of successively higher strength hot spots (Figure 5(f)). The hot spot formed after the collapse of the elongated void is thereby able to initiate chemical reaction (Figure 5(h)). This self-strengthening mechanism of the shock is present only in the elongated void situation and not present in the collapse of cylindrical voids. Therefore, for a given void area the elongated void is more sensitive than a corresponding cylindrical void.

### C. Effect of orientation of elongated voids on sensitivity of pressed energetic materials

The real meso-structure of pressed energetic materials (Figure 1) contains elongated voids of various orientations and aspect ratios. The orientation of elongated voids can significantly affect the sensitivity behavior of energetic materials, as indicated in the work of Levesque et al. [8] Therefore, the next part of this study seeks to quantify the effect of orientation of elongated voids on ignition threshold of energetic materials and to obtain physical insights into the effect of orientation. The computational setup shown in Figure 2 is used to study the effect of orientation. The orientation is prescribed with respect to the incident shock wave. Five different orientations are considered i.e.  $\theta = 0^\circ, 30^\circ, 45^\circ, 60^\circ$  and  $90^\circ$ . The void thickness and length are maintained constant for all the orientations (Figure 2). The shock pulse duration is maintained at  $0.5\text{ ns}$ . As shown in section IV.B.1 the threshold for the elongated void oriented at an angle of  $\theta = 45^\circ$  lies between  $500\text{ m/s}$  and  $650\text{ m/s}$ . Based on this observation a shock strength of  $650\text{ m/s}$  is used in the current analysis to examine relative sensitivity of other orientations. Figure 6 shows the time variation of the total specific internal energy and the volume averaged mass fraction of the final gaseous species for the five orientations. It can be seen that for the elongated voids oriented at angles of  $\theta = 0^\circ, 30^\circ$  and  $45^\circ$ , there is sharp rise in the total specific internal energy (due to sustained chemical reactions) after the initial peak generated by the collapse of the elongated voids (Figure 6(a)). Also, the volume mass fraction of the final gaseous species increases and reaches the value of 1 indicating complete burning in the material (Figure 6(b)). For elongated voids oriented at angles of  $\theta = 60^\circ$  and  $90^\circ$  the strength of the hot spot formed after the collapse of the elongated void is not sufficient to initiate reaction

and the hot spot is quenched. This is indicated in the total specific internal energy plot (Figure 6(a)). Therefore, the critical orientations for which an elongated void are sensitive lie between  $0^\circ$  and  $45^\circ$  for the given loading conditions.

Next, we seek to understand why the elongated voids oriented at angle that lie between  $0^\circ - 45^\circ$  are more sensitive than other orientations. Figure 7 shows the comparison between the temperature fields generated during collapse of voids oriented at angles of  $0^\circ$  and  $90^\circ$ . The major axis of the  $0^\circ$  void aligns with the direction of the shock travel (Figure 7(a)) as compared to the  $90^\circ$  void where it is perpendicular to the direction of shock travel (Figure 7(b)). For the  $0^\circ$  void, the incident shock causes a pinching action and generates high temperature hot spots (Figure 7(c)). For the  $90^\circ$  void, the shock impacts the upstream surface of the void and reflects back as a rarefaction wave (Figure 7(d)). The rarefaction wave cools down the hot spot formed after the collapse and no reaction is observed for the  $90^\circ$  void. The rarefaction effect is not present for the  $0^\circ$  void as the shock wave propagation aligns with the length of the void (Figure 7(g)). This observation is in agreement with Levesque and Vitello [8] where it is shown that elongated shapes aligned with the direction of shock propagation cause the formation of stronger hot spots.

As the orientation of the void is increased from  $0^\circ$  towards  $90^\circ$  the ability of the rarefaction wave to cool the hot spot also increases. Figure 8 shows this effect by comparing the temperature contour plots for three other orientations viz.  $30^\circ$ ,  $45^\circ$  and  $60^\circ$ . The pinching mechanism of the void collapse to produce higher strength hot spots dominates until the orientation reaches  $45^\circ$ . This causes reaction initiation for the  $30^\circ$  (Figure 8(j)) and the  $45^\circ$  void (Figure 8(k)). With further increase in orientation to  $60^\circ$ , the rarefaction effect dominates and cools down the hot spot thereby preventing reaction initiation (Figure 8(l)). There is therefore a competition between the pinching mechanism of the void and the rarefaction-induced cooling during the collapse of elongated voids; as the orientation increases towards  $90^\circ$  the rarefaction effect tends to dominates. The pinching mechanism dominates for the orientation of less than  $45^\circ$  causing the voids to be more sensitive in the range of  $0 - 45^\circ$ .

#### **D. Effect of aspect ratio of elongated voids on sensitivity**

The previous cases analyzed the effect of the void orientation on the sensitivity of HMX. Along with the orientation the aspect ratio of an elongated void can affect the sensitivity of the porous energetic materials. The aspect ratio in the context of current analysis is defined as the ratio of length of the void to its thickness as illustrated in Figure 2. The aspect ratio for the elongated void shown in Figure 2 is 20. The orientation of the void with respect to the incident shock wave is kept constant at  $\theta = 45^\circ$ . The shock loading with imposed particle speed of  $650 \text{ m/s}$  and pulse duration of  $0.5 \text{ ns}$  is applied from the west face of the boundary. The shock strength of  $650 \text{ m/s}$  is used in the current analysis because the ignition threshold for the elongated void with aspect ratio of 20 and oriented at an angle of  $45^\circ$  was observed to lie between  $500 \text{ m/s}$  and  $650 \text{ m/s}$ . The aspect ratio of the void is varied by keeping the void area constant at  $5 \mu\text{m}^2$ . Six different aspect ratios are used corresponding to 2, 3, 5, 10, 15 and 20.

Figure 9 shows the time variation of the total specific internal energy and the volume averaged mass fraction of the final gaseous species for all the six void geometries. For the same void volume fraction and shock loading, the voids with smaller aspect ratios, i.e. less than 5, do

not produce sustained reactions and the hot spot formed from the collapse of the void quenches. This can be seen in Figure 9, where the total specific internal energy rises because of the formation of the hot spot and eventually settles down to a constant value. Also, the mass fraction of the gaseous species does not increase with time indicating non-reactive cases. For the voids with aspect ratios greater than 5, the hot spot formed after the collapse leads to the initiation of chemical reactions indicated by the sharp rise in the total specific internal energy (Figure 9(a)). Also, the mass fraction of the gaseous species increases and reaches the value of 1 showing ignition and complete burning of the HMX material (Figure 9(b)). Therefore, thicker voids (low aspect ratios) are less sensitive than thinner voids (large aspect ratio). The critical aspect ratio lies above the value of 5 for the given loading conditions and void orientation. Note that the critical aspect ratio will depend on shock loading as well as on orientation.

In the above simulations, thicker voids are found to be less sensitive than thinner voids. Figure 10 and Figure 11 seek to understand the mechanisms underlying this observation by showing the deformation profile of voids of different aspect ratios. Figure 10 compares the time variation of the temperature contour plots of voids with aspect ratio of 2 and 10. The void with aspect ratio of 2 undergoes collapse by the formation of an asymmetrical material jet (Figure 10(c) and Figure 10(e)). The void with aspect ratio of 10 undergoes collapse by the pinching mechanism leading to the successive collapse of the void. It was shown in the section IV.B.3 that the pinching mechanism produces higher temperature hot spots than the collapse under material jetting by comparing the behavior of a cylindrical and an elongated void. This difference in the mode of collapse, i.e. jetting versus pinching, causes the sensitivity of thicker voids to be low when compared to the thin voids.

The physical mechanism governing the collapse of elongated voids transitions from material jetting to pinching mechanism as the aspect ratio of the void is increased. This transition is demonstrated in Figure 11 by comparing the numerical Schlieren plots for three aspect ratios viz. 2, 5 and 10. The void with aspect ratio of 2 deforms because of the formation of a material jet (Figure 11(d)). The shock focusing due to the jet increases as the deformation of the void progresses (Figure 11(g)) leading to final collapse (Figure 11(j)). When the aspect ratio is increased to 5, initially the void starts to deform but there is no pinching action involved at the start of void collapse (Figure 11(e)). As the void starts to deform further the pinching action comes into play (Figure 11(h)) leading to the complete collapse of the void. Further increasing the aspect ratio to 20 causes the void to collapse because of the pinching mechanism (Figure 11(f)) and successive pinching events continue till the void is collapsed completely (Figure 11(i)). It can be seen that the transition of the physical mechanism from material jetting to pinching takes place as the aspect ratio is increased. Voids of aspect ratio of 5 can be identified as the threshold where this transition is most evident. For thicker voids, the surface area of the void that interacts with the incident shock initially is high which allows sufficient time for the formation of a material jet. For thinner voids, the surface area impacted by the incident shock wave is small causing the immediate collapse by a pinching action. The series of pinching actions creates a high strength hot spot and makes the thinner voids more sensitive.

### **E. Shock analysis of Class III pressed explosive sample**

The current study has identified the key morphological features of elongated voids that cause the voids to exhibit greater sensitivity. The insights obtained from the numerical experiments above, with regular (analytical)-shaped elongated voids, can help to understand the initiation behavior of real (imaged) pressed explosive samples (Figure 1). This can also help in the development of the ability to predict the locations in the pressed samples where critical hot spots can occur. To demonstrate this, shock simulations of the Class III pressed HMX sample (shown in Figure 1(a)) are performed.

Figure 12 shows the computational setup for the analysis of the Class III sample. Shock loading of strength  $1000\text{ m/s}$  and pulse duration  $0.5\text{ ns}$  is applied from the west face of the domain. The other faces of the domain boundary are modeled as outlet boundaries. The SEM image of the Class III sample is processed using the image processing algorithms implemented in SCIMITAR3D [10,23]. Speckle reducing anisotropic diffusion is used to denoise the image and active contouring algorithm is used for image segmentation to obtain a level set representation of the voids present in the meso-structure. The image processing algorithms have been presented in detail and validated in previous work [10,23].

Based on the simulations above, the critical orientation lies between  $0^\circ$  and  $45^\circ$ ; and the critical aspect ratio is greater than 5. In Figure 12, a small number of voids that lie outside these mentioned range of orientations and aspect ratios are tagged (numbered 1-4 in Figure 12). The void at location 1 is oriented approximately at an angle of  $30^\circ - 45^\circ$ , at location 2 it is oriented at an angle of  $20^\circ - 30^\circ$ , at location 3 the void is oriented at an angle between  $50^\circ - 70^\circ$ , the void at location 4 is oriented at angle of  $135^\circ$  ( $-45^\circ$ ) with respect to shock wave. All the four voids have high aspect ratios (i.e. they are thin voids). It will be shown that in this particular meso-structure of Class III, the voids that have high aspect ratio and orientation play a key role in affecting the sensitivity of the sample to shock loading.

The voids at locations 1,2 and 4 lie in the critical parameter range of orientation and aspect ratio; it can be expected that these are some of the critical locations where reaction will initiate. Void 3 lies outside the critical parameter range of orientation and it may be less sensitive. Shock analysis on the Class III sample is performed to understand how closely the predictions hold up for all the four locations. The grid resolution is decided based on the elongated void grid resolution study in section IV.A i.e. 40 grid points are used across the void thickness. The void at location 1 is selected as a standard to maintain the grid resolution requirement in the full domain. Note that the void at location 1 was resolved by roughly 5 pixels across its thickness in the original SEM image. Therefore, by refining the computational grid by a factor of 8 times the original image resolution 40 grid points across the void thickness was employed to enable reliable computations of the collapse.

Figure 13 shows the numerical Schlieren plots at different instances of shock propagation showing the local deformation of voids and the formation of blast waves from successive collapse of the voids. The void at location 1 starts to collapse and due to the pinching action high strength blast waves (Figure 13(b) and Figure 13(c)) emanate from the collapse locations. The same is observed for the voids at location 2 and 4 (Figure 13(d) and Figure 13(f)). The collapse of the other voids surrounding void 2 causes the formation of a blast wave and there is a complex interaction of the blast waves formed from all the voids. This suggests strong void-void interactions between all the neighboring voids as noted in the work of Kapahi and Udaykumar



[7] in the context of cylindrical voids. The void at location 3 also collapses but as can be seen in Figure 13(f) but the blast wave strength formed from its collapse is not sufficiently high and no reaction initiates at that location.

The reaction initiation and sensitivity of each of the 4 voids are elucidated using contour plots of the temperature and the mass fraction of final gaseous species (Figure 14). Based on the predictions from the numerical experiments the voids at location 1, 2 and 4 are categorized as sensitive and the void at location 3 void is less sensitive. The void at location 1 creates a hot spot of sufficient strength and reaction initiates (Figure 14(c)) locally at location 1. The reaction initiation can also be seen in the contour plot of the mass fraction of the gaseous species (Figure 14(d)). The same is observed for the voids at location 2 (Figure 14(e) and Figure 14(f)) and 4 (Figure 14(g) and Figure 14(h)). The void at location 3 does not lead to the formation of a high strength hot spot and no reaction initiation is observed at that location (Figure 14(e) and Figure 14(f)). The behavior of all the 4 voids in this real meso-structure is consistent with the predictions from the numerical experiments of idealized single elongated voids.

## V. CONCLUSIONS

Using reactive meso-scale simulations this work analyzes the sensitivity behavior of elongated voids which are prevalent in real meso-structures of pressed explosives. The effect of void orientations and aspect ratios on reaction initiation is studied. The understanding developed from the numerical simulations is shown to be useful in the prediction of reaction initiation and ignition locations in real meso-structures of pressed explosives. This is demonstrated by performing meso-scale analysis of a given sample of coarse grain pressed explosives categorized as Class III explosives. The key observations and insights obtained from the current work are itemized as follows:

- 1) It is shown that coarse grids under-predict the hot spot temperatures and can lead to incorrect ignition threshold predictions. In general, 40 grid points across the elongated void thickness were found to be adequate to obtain a converged solution for an accurate reactive meso-scale simulation.
- 2) It is shown that elongated voids are more sensitive and generate higher strength hot spots when compared to cylindrical voids. This difference in the behavior of cylindrical and elongated void is connected to the physical mechanisms governing the collapse of voids of different shapes. Cylindrical voids collapse under the application of shock load leading to formation of material jet. Elongated voids collapse by a pinching mechanism leading to the subsequent collapse of one surface of the void on the opposing surface. Each pinching instance generates blast waves. As the collapse progresses along the length of the void, the blast waves intensify and cause the formation of high strength hot spots. This self-strengthening mechanism is not present in the situation involving a cylindrical void which makes it less sensitive when compared to elongated voids.
- 3) Elongated voids of various orientations and aspect ratios are present in the real meso-structure of the pressed explosives. It is shown that voids oriented at an angle less than  $45^\circ$  with respect to the incident shock wave are more sensitive. There are two competing mechanisms that operate

during the collapse of arbitrarily oriented elongated voids: pinching mechanisms causing the collapse of the voids and rarefaction effects because of the shock reflection from the free surface of the voids when the incident shock impacts it. For orientations less than  $45^\circ$  the pinching mechanism dominates over the rarefaction effects and causes the voids to be sensitive.

4) Elongated voids of aspect ratio greater than or equal to 5 are found to be more sensitive when compared to the low aspect ratio voids. Material jetting is the primary collapse mechanism that causes the collapse of the low aspect ratio i.e. thicker voids. The self-strengthening pinching mechanism is the governing mechanism for the collapse of high aspect ratio voids i.e. thinner voids, which makes the high aspect ratio void more sensitive.

The understanding of the sensitivity behavior of elongated voids is applied to predict critical void locations in the real meso-structure of a Class III pressed explosive samples. The prediction of which voids are most sensitive can be made fairly robustly on the basis on their orientation and aspect ratio. This work therefore enables insights and physical mechanisms derived from meso-scale simulations to be used to predict the behavior of real meso-scale geometries.

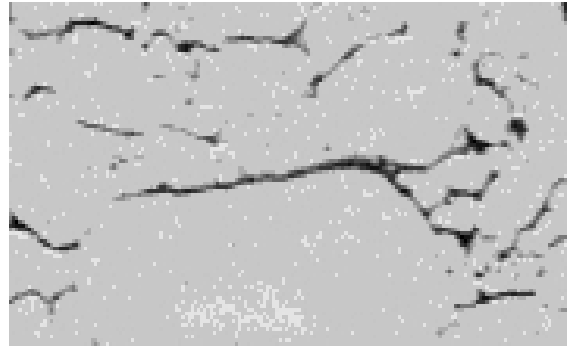
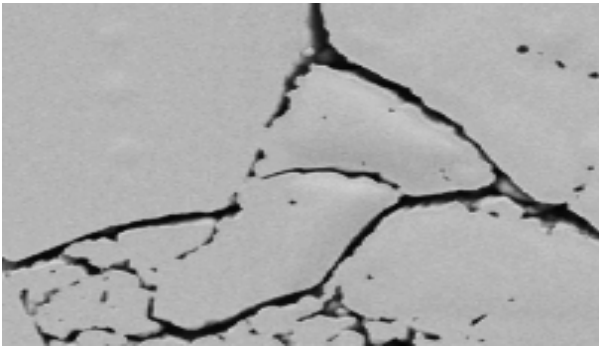
The current work enhances the understanding of the behavior of pressed explosives under certain assumptions and limitations. The voids are modeled in two dimensions whereas it is important to understand 3D effects on the sensitivity behavior of elongated voids. A preliminary attempt to distinguish 2D versus 3D physics of void collapse was presented in previous work [9]. 3D effects will be considered further in the future work. Also, the current work demonstrates that the numerical experiments on elongated voids can predict critical locations for initiation in a real meso-structure. Meso-scale computations of real meso-structures are expensive. Therefore, it may be advantageous to develop an approach that can quantify the sensitivity of a given meso-scale sample by correlating sensitivity with meso-scale morphology. This requires a framework to quantify the local meso-structural morphological features in a given sample. To this end, ongoing work is aimed at developing an image analysis tool that can quantify global morphological metrics (particle size, shape and proximity distributions) and local metrics (void orientations, aspect ratios, correlation functions) and to relate the morphological metrics to sample sensitivity.

## **VI. ACKNOWLEDGEMENT**

This work was performed under grants from the AFOSR Computational Mathematics program (Program Manager: Dr. Jean-Luc Cambier), AFOSR Energetics Materials Program (Program manager : Dr. Jennifer Jordan) and from the AFRL-RWPC (Computational Mechanics Branch, Eglin AFB)).

- [1] Welle, E. J., Molek, C. D., Wixom, R. R., and Samuels, P., 2014, "Microstructural Effects on the Ignition Behavior of HMX," *Journal of Physics: Conference Series*, IOP Publishing, p. 052049.
- [2] Khasainov, B. A., Borisov, A. A., Ermolaev, B. S., and Korotkov, A. I., 1981, "Two-Phase Visco-Plastic Model of Shock Initiation of Detonation in High Density Pressed Explosives," *7th Symposium (International) on Detonation, Annapolis, MD*, pp. 435–447.
- [3] Field, J. E., 1992, "Hot Spot Ignition Mechanisms for Explosives," *Acc. Chem. Res.*, **25**(11), pp. 489–496.
- [4] Menikoff, R., 2004, "Pore Collapse and Hot Spots in HMX," *AIP Conference Proceedings*, IOP INSTITUTE OF PHYSICS PUBLISHING LTD, pp. 393–396.
- [5] Tran, L., and Udaykumar, H. S., 2006, "Simulation of Void Collapse in an Energetic Material, Part I: Inert Case," *J. Propuls. Power*, **22**(5), pp. 947–958.
- [6] Tran, L., and Udaykumar, H. S., 2006, "Simulation of Void Collapse in an Energetic Material, Part 2: Reactive Case," *J. Propuls. Power*, **22**(5), pp. 959–974.
- [7] Kapahi, A., and Udaykumar, H. S., 2013, "Dynamics of Void Collapse in Shocked Energetic Materials: Physics of Void–void Interactions," *Shock Waves*, **23**(6), pp. 537–558.
- [8] Levesque, G. A., and Vitello, P., 2015, "The Effect of Pore Morphology on Hot Spot Temperature," *Propellants Explos. Pyrotech.*, **40**(2), pp. 303–308.
- [9] Kapahi, A., and Udaykumar, H. S., 2015, "Three-Dimensional Simulations of Dynamics of Void Collapse in Energetic Materials," *Shock Waves*, **25**(2), pp. 177–187.
- [10] Rai, N. K., and Udaykumar, H. S., 2015, "Mesoscale Simulation of Reactive Pressed Energetic Materials under Shock Loading," *J. Appl. Phys.*, **118**(24), p. 245905.
- [11] Kapila, A. K., Schwendeman, D. W., Gambino, J. R., and Henshaw, W. D., 2015, "A Numerical Study of the Dynamics of Detonation Initiated by Cavity Collapse," *Shock Waves*, pp. 1–28.
- [12] Springer, H., Tarver, C., and Bastea, S., 2015, "Effects of High Shock Pressures and Pore Morphology."
- [13] Swantek, A. B., and Austin, J. M., 2010, "Collapse of Void Arrays under Stress Wave Loading," *J. Fluid Mech.*, **649**, pp. 399–427.
- [14] Bourne, N. K., and Field, J. E., 1991, "Bubble Collapse and the Initiation of Explosion," *Proc. R. Soc. Lond. Math. Phys. Eng. Sci.*, **435**(1894), pp. 423–435.
- [15] Bourne, N. K., and Milne, A. M., 2003, "The Temperature of a Shock-Collapsed Cavity," *Proc. R. Soc. Lond. Math. Phys. Eng. Sci.*, **459**(2036), pp. 1851–1861.
- [16] Sambasivan, S., Kapahi, A., and Udaykumar, H. S., 2012, "Simulation of High Speed Impact, Penetration and Fragmentation Problems on Locally Refined Cartesian Grids," *J. Comput. Phys.*

- [17] Kapahi, A., Sambasivan, S., and Udaykumar, H. S., 2013, "A Three-Dimensional Sharp Interface Cartesian Grid Method for Solving High Speed Multi-Material Impact, Penetration and Fragmentation Problems," *J. Comput. Phys.*, **241**, pp. 308–332.
- [18] Kulikovskii, A. G., Pogorelov, N. V., and Semenov, A. Y., 2000, *Mathematical Aspects of Numerical Solution of Hyperbolic Systems*, CRC Press.
- [19] Rai, N. K., Schmidt, M., and UdayKumar, H. S., "High Resolution Simulations of Cylindrical Void Collapse in Energetic Materials: Effect of Primary and Secondary Collapse on Initiation Thresholds," *Physcal Rev. Fluids* Submitted.
- [20] Shu, C.-W., and Osher, S., 1989, "Efficient Implementation of Essentially Non-Oscillatory Shock-Capturing Schemes, II," *J. Comput. Phys.*, **83**(1), pp. 32–78.
- [21] Osher, S., 1988, "Fronts Propagating with Curvature Dependent Speed Algorithms Based on Hamilton-Jacobi Formulations," *J. Comput. Phys.*, **79**, pp. 12–49.
- [22] Fedkiw, R. P., Aslam, T., Merriman, B., and Osher, S., 1999, "A Non-Oscillatory Eulerian Approach to Interfaces in Multimaterial Flows (the Ghost Fluid Method)," *J. Comput. Phys.*, **152**(2), pp. 457–492.
- [23] Dillard, S. I., Mousel, J. A., Shrestha, L., Raghavan, M. L., and Vigmostad, S. C., 2014, "From Medical Images to Flow Computations without User-Generated Meshes," *Int. J. Numer. Methods Biomed. Eng.*, **30**(10), pp. 1057–1083.



(a) Class III pressed energetic material sample (b) Class V pressed energetic material

Figure 1: SEM image of the meso-structure of the pressed explosives samples. Two different types of pressed explosives are shown; these are Class III and Class V explosive samples. Class III is a coarse grain explosive and Class V is fine grain.

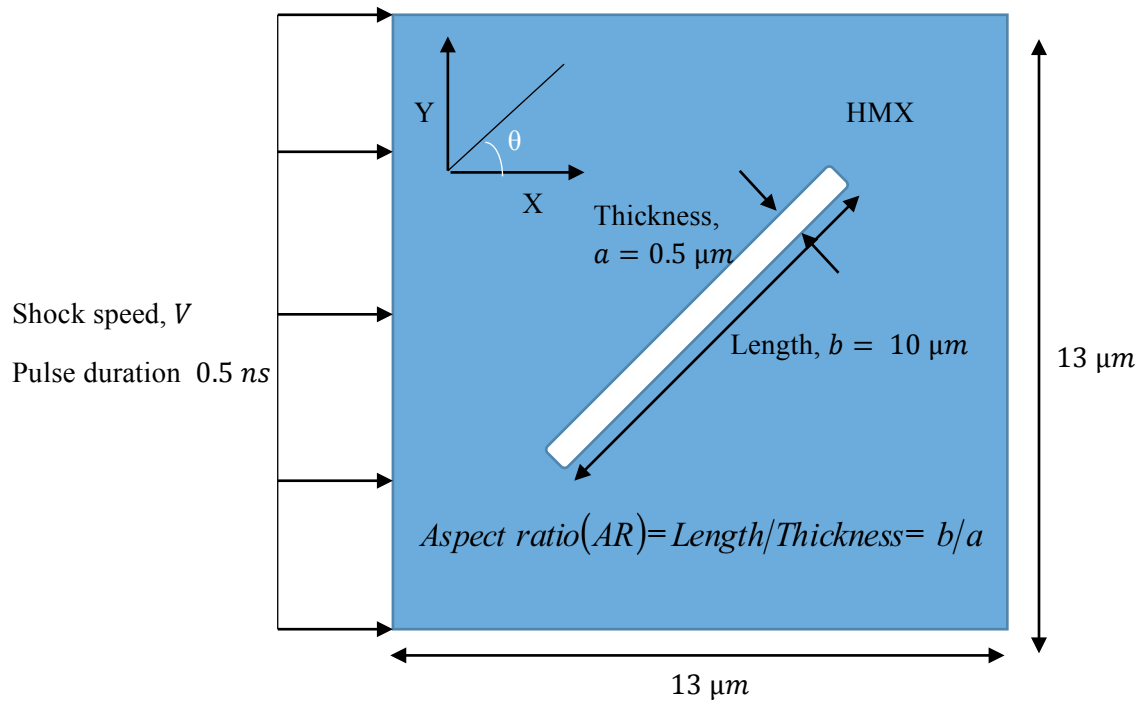


Figure 2: Computational setup for the meso-scale simulations of the elongated void. An elongated void with thickness  $a = 0.5 \mu\text{m}$  and length  $b = 10 \mu\text{m}$  is oriented at angle  $\theta$  with respect to the incident shock wave. Shock load of prescribed particle speed and pulse duration of  $0.5 \text{ ns}$  is applied from the west face of the domain boundary. East, south and north faces are modeled as outlet conditions.

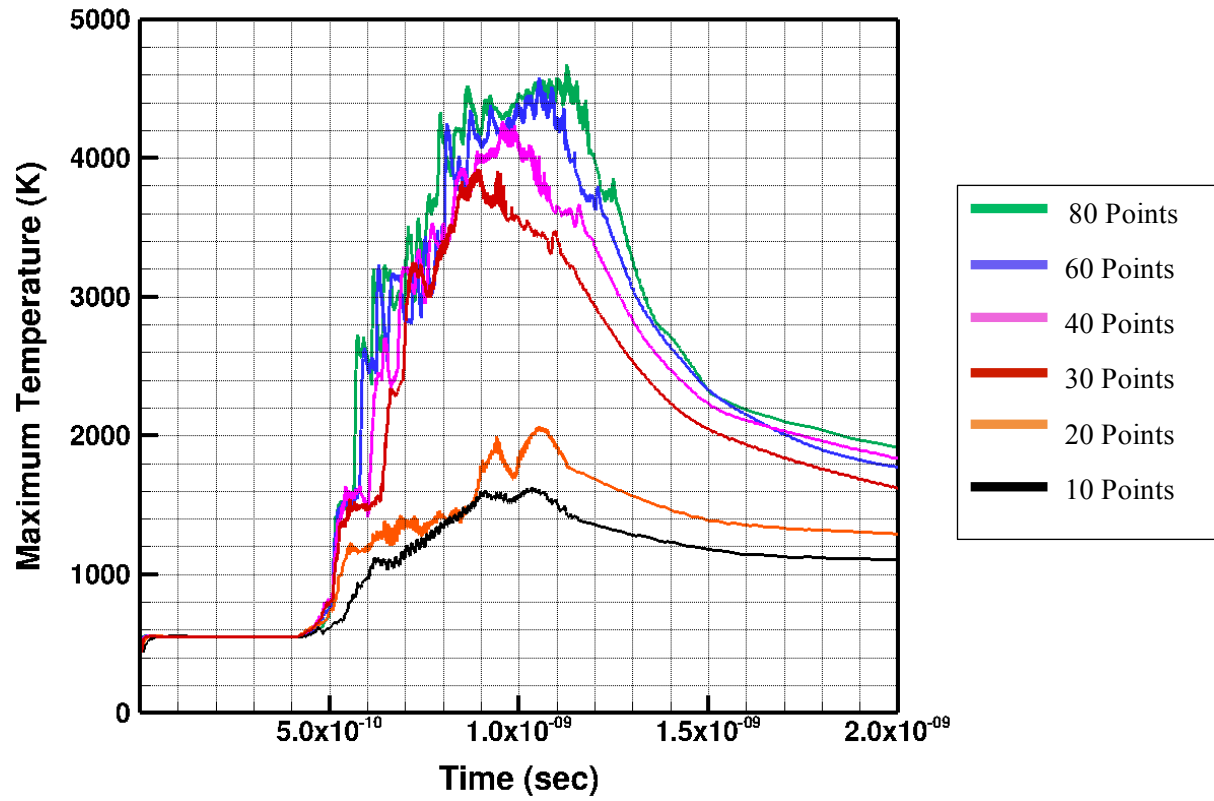
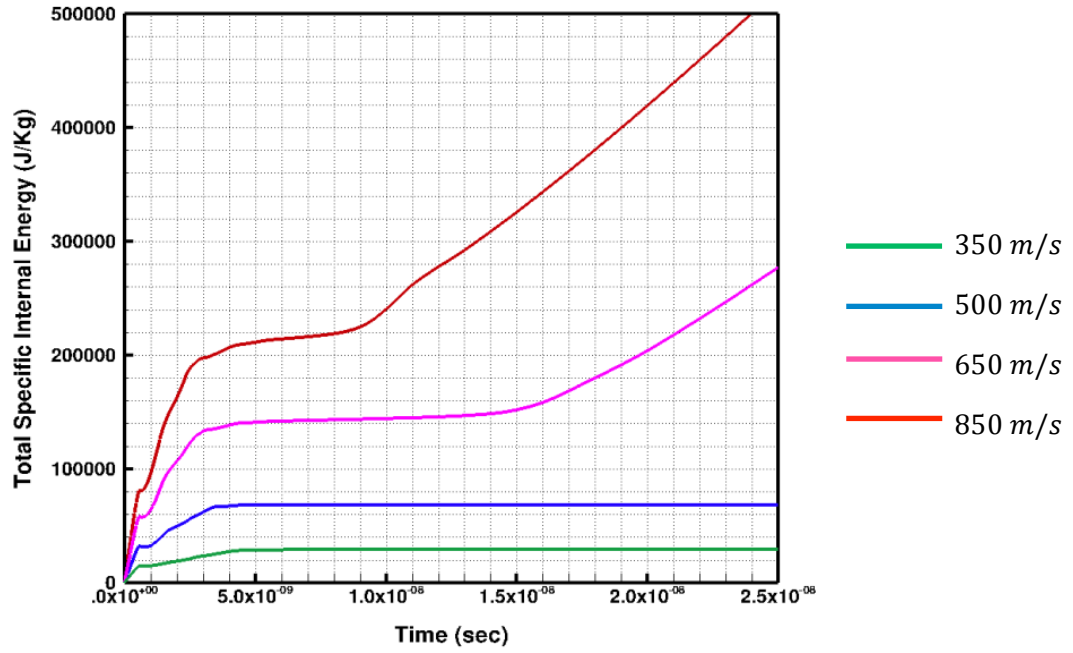
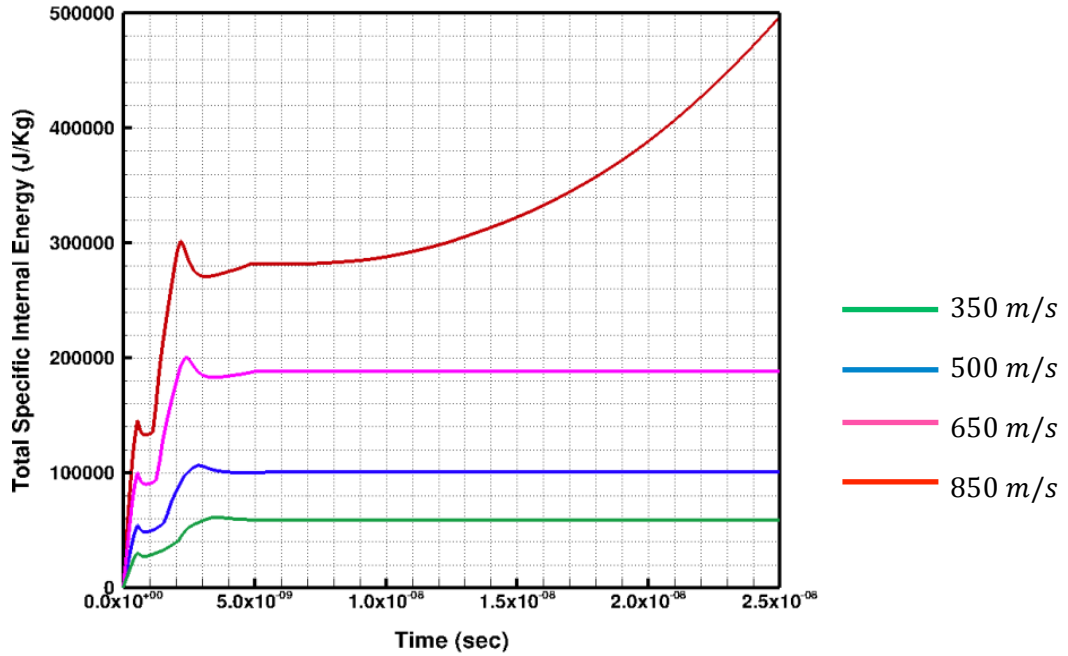


Figure 3: Grid convergence study for the inert void collapse simulation. The study is performed for a single elongated void of thickness  $0.5\ \mu\text{m}$  and length  $20\ \mu\text{m}$  in HMX material under the shock loading of  $1000\ \text{m/s}$ . Six different grid sizes corresponding to 10, 20, 30, 40, 60 and 80 grid points across the void thickness are considered.



(a) Time variation of the total specific internal energy for elongated void for different shock strengths



(b) Time variation of total specific internal energy for the circular void for different shock strengths

Figure 4: Time variation of the total specific internal energy for different shock strengths of imposed particle speed of 350, 500, 650 and 850  $m/s$ . The results are obtained from the reactive meso-scale simulation of an elongated void (Figure 2) oriented at angle of  $45^\circ$  with respect to the incident shock wave (Figure 4(a)) and a circular void of same area as elongated void. The diameter of the circular void is  $2.52 \mu m$ . The loading pulse is kept constant at  $0.5 ns$  for all the simulations.



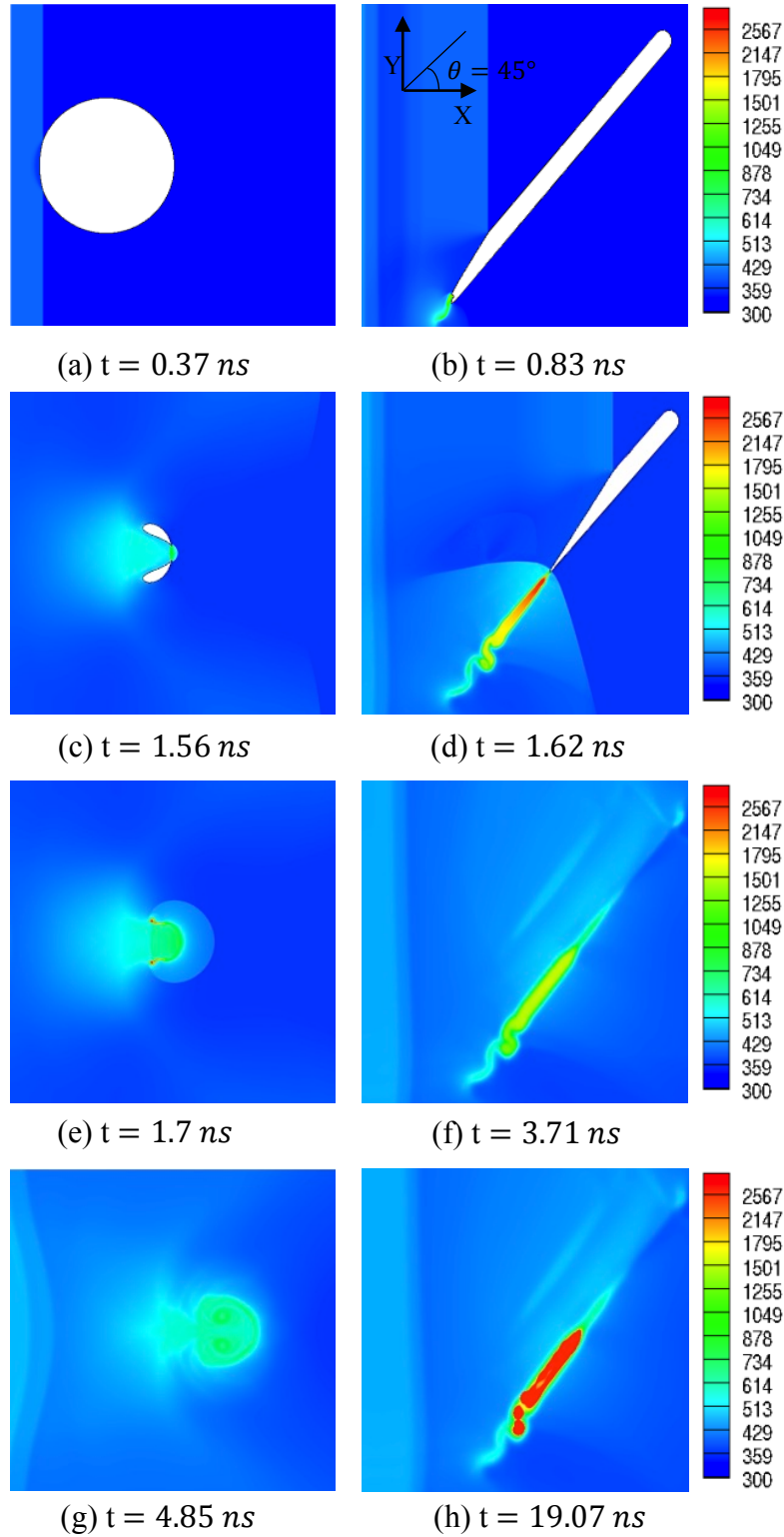
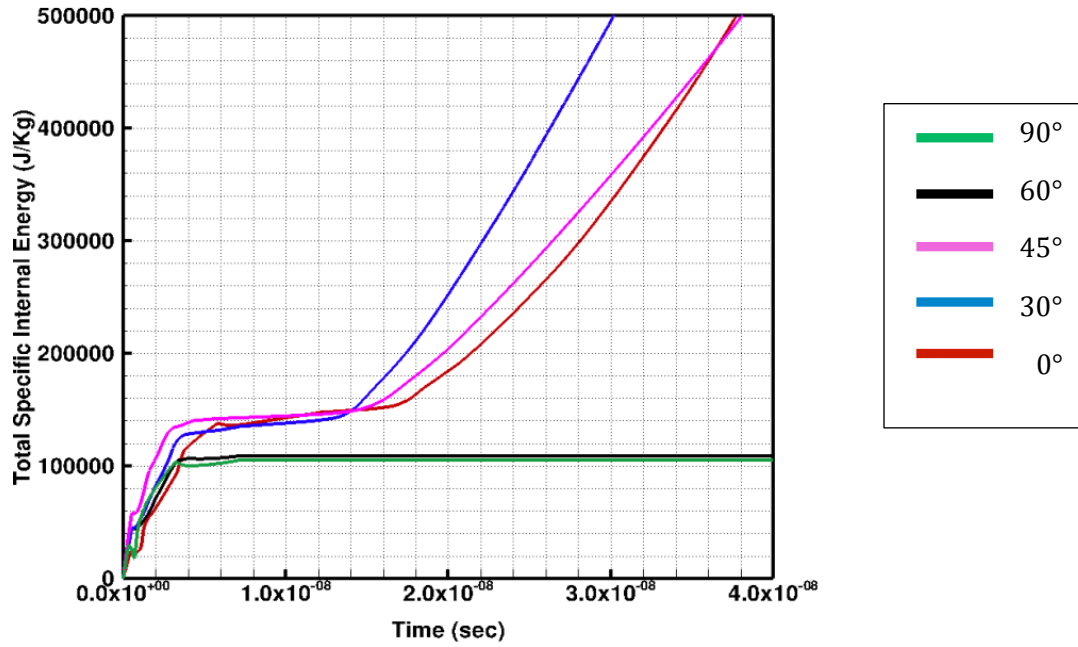
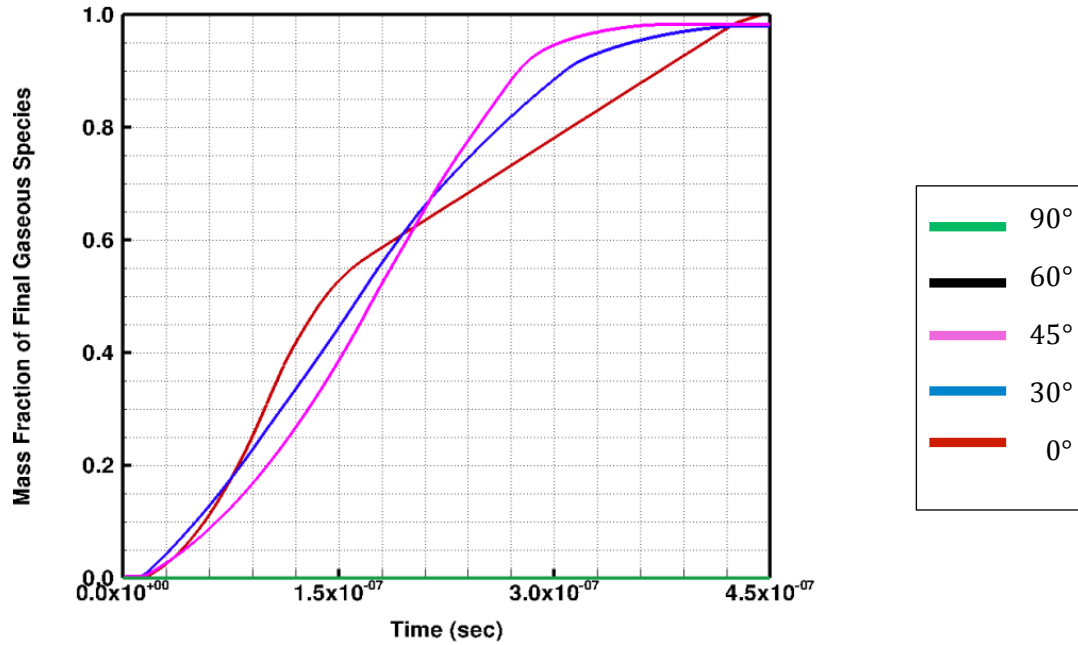


Figure 5: The contour plots of temperature (K) at different instants of time for the reactive meso-scale simulations of a cylindrical void and an elongated void oriented at an angle of  $45^\circ$  with respect to the incident shock load. The elongated void is  $0.5 \mu\text{m}$  thick and  $10 \mu\text{m}$  long. The diameter of the cylindrical void is  $2.52 \mu\text{m}$ . The void area of the elongated void and the cylindrical void is same. The shock load of particle speed  $650 \text{ m/s}$  and pulse duration of  $0.5 \text{ ns}$  is applied from the west face of the domain.



(a) Time variation of the total specific internal energy



(b) Time variation of the volume averaged mass fraction of the gaseous species

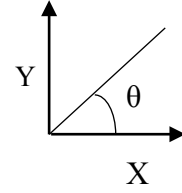
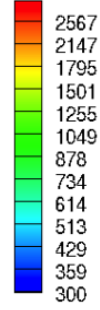
Figure 6: Time variation of the total specific internal energy and volume averaged mass fraction of the gaseous species for different shock strengths of  $650 \text{ m/s}$  and pulse duration of  $0.5 \text{ ns}$ . The results are obtained from the reactive meso-scale simulation of an elongated void (Figure 2). The effect of orientation of the elongated void is studied by studying 5 different orientations  $0^\circ, 30^\circ, 45^\circ, 60^\circ, 90^\circ$ . The orientation is prescribe with respect to the incident shock wave.



(a)  $\theta = 0^\circ$  void at  $t = 0.68 \text{ ns}$



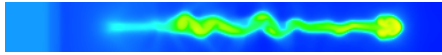
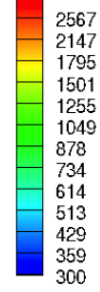
(b)  $\theta = 90^\circ$  void at  $t = 0.45 \text{ ns}$



(c)  $t = 1.37 \text{ ns}$



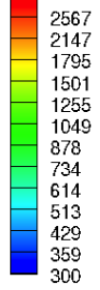
(d)  $t = 0.73 \text{ ns}$



(e)  $t = 11.58 \text{ ns}$



(f)  $t = 1.2 \text{ ns}$



(g)  $t = 86.3 \text{ ns}$



(h)  $t = 2.32 \text{ }\mu\text{s}$

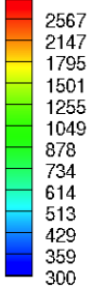


Figure 7: Temperature (K) contour plots at different instants of time showing the difference in the reaction initiation behavior of two elongated voids of thickness  $0.5 \text{ }\mu\text{m}$  and length  $10 \text{ }\mu\text{m}$  oriented at angle of  $0^\circ$  and  $90^\circ$  with respect to the shock load. The shock speed for the analysis is maintained at  $650 \text{ m/s}$  and the pulse duration is  $0.5 \text{ ns}$ .

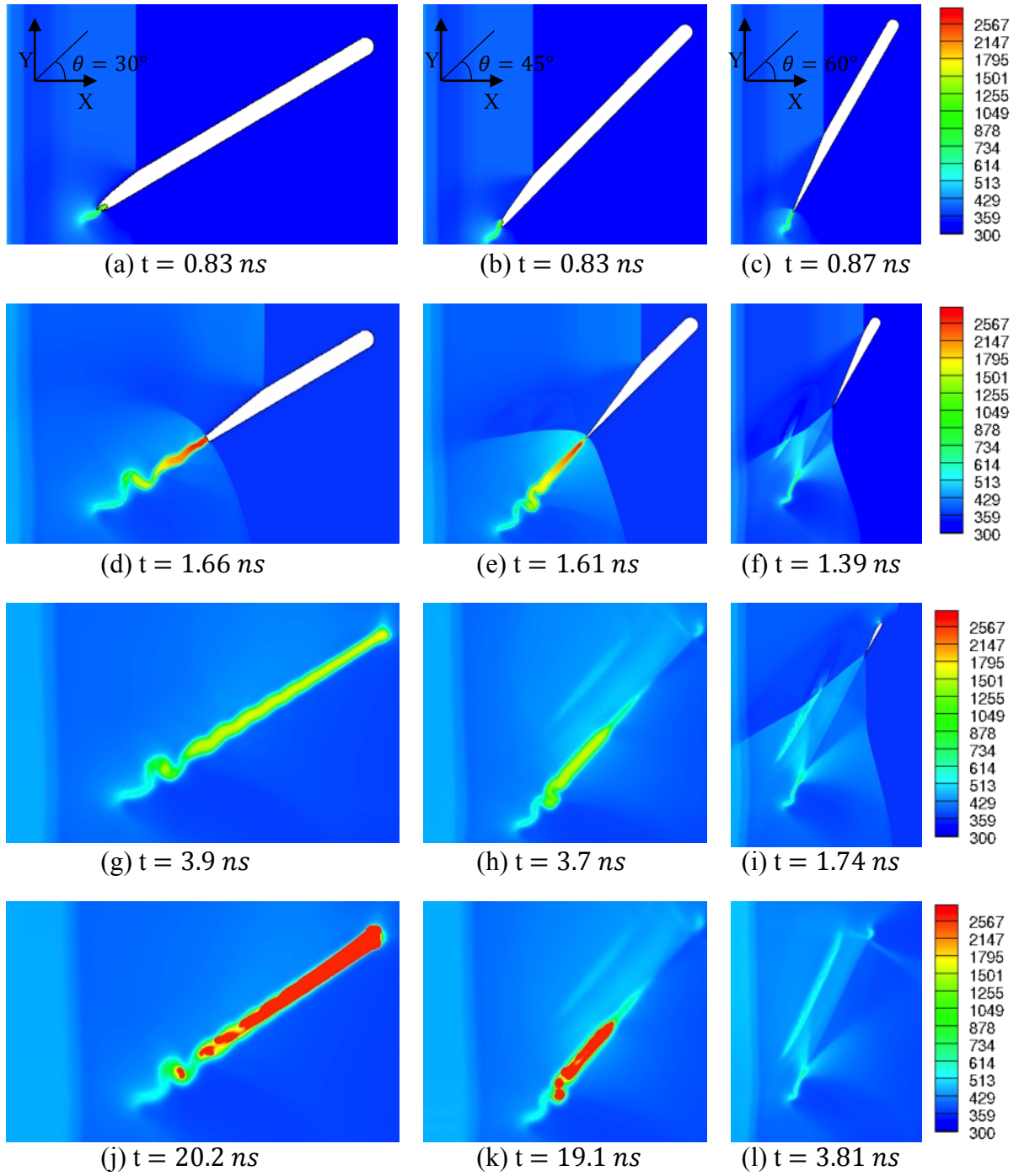
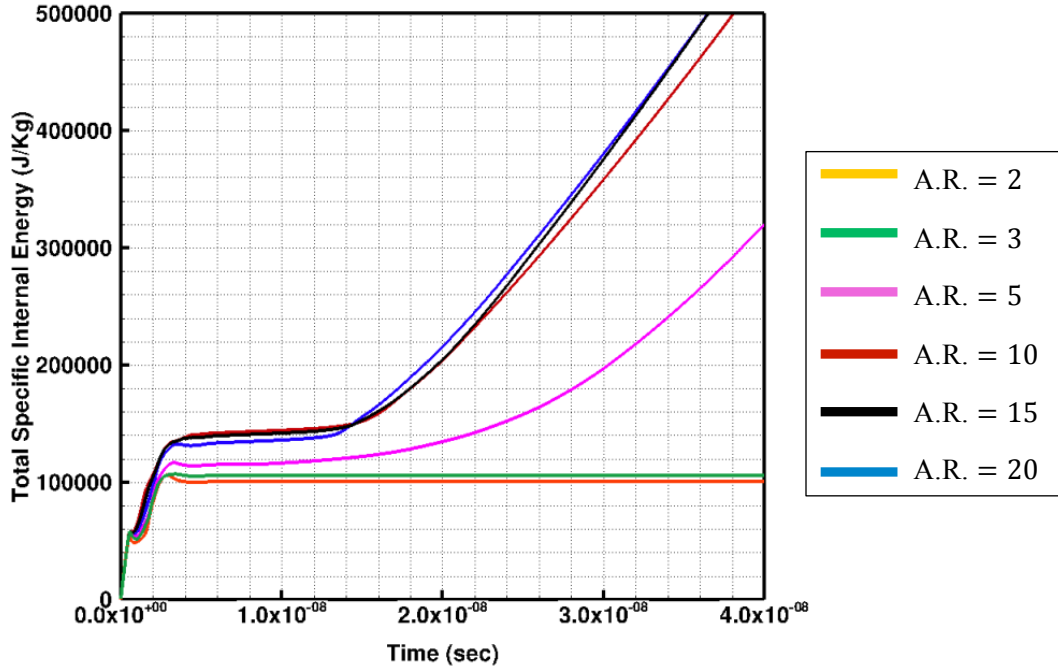
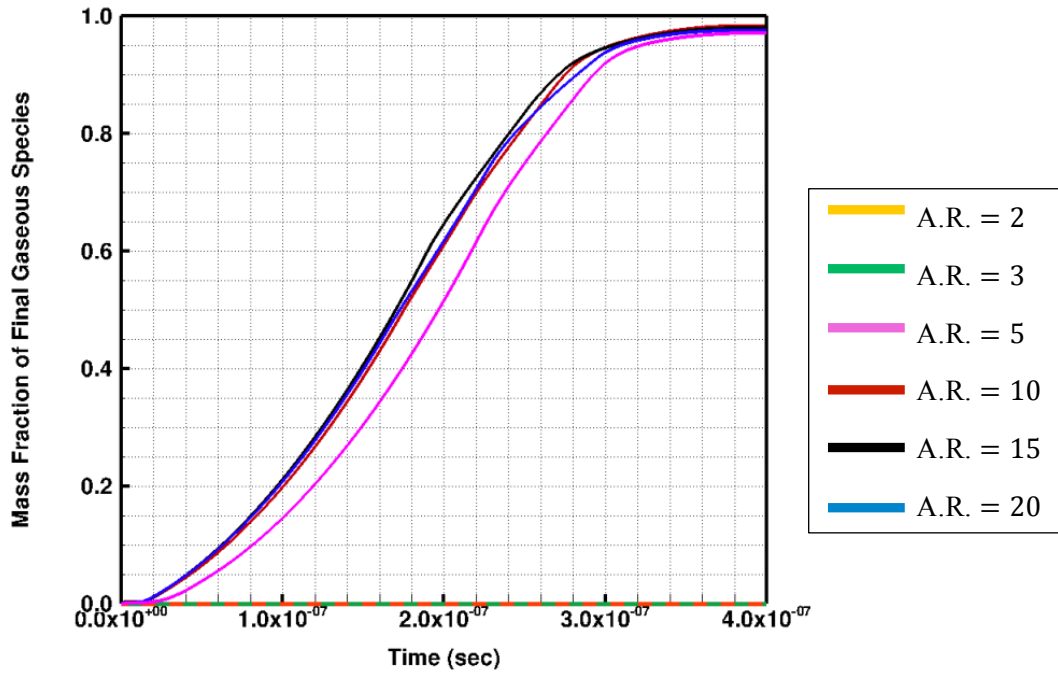


Figure 8: Temperature (K) contour plots at different instants of time showing the difference in the reaction initiation behavior of three elongated voids of thickness  $0.5 \mu\text{m}$  and length  $10 \mu\text{m}$  oriented at angle of  $30^\circ$ ,  $45^\circ$  and  $60^\circ$  with respect to the shock load. The shock speed for the analysis is maintained at  $650 \text{ m/s}$  and the pulse duration is  $0.5 \text{ ns}$ .



(a) Time variation of the total specific internal energy



(b) Time variation of the volume averaged mass fraction of the gaseous species

Figure 9: Time variation of the total specific internal energy and volume averaged mass fraction of the gaseous species for different shock strengths of 650 m/s and pulse duration of 0.5 ns. The results are obtained from the reactive meso-scale simulation of an elongated void (Figure 4) oriented at an angle of  $45^\circ$  with respect to the incident shock wave. The effect of orientation of the elongated void is studied by studying 6 different aspect ratio's (AR) of value 2, 3, 5, 10, 15 and 20. AR is defined as the ratio of length by thickness.

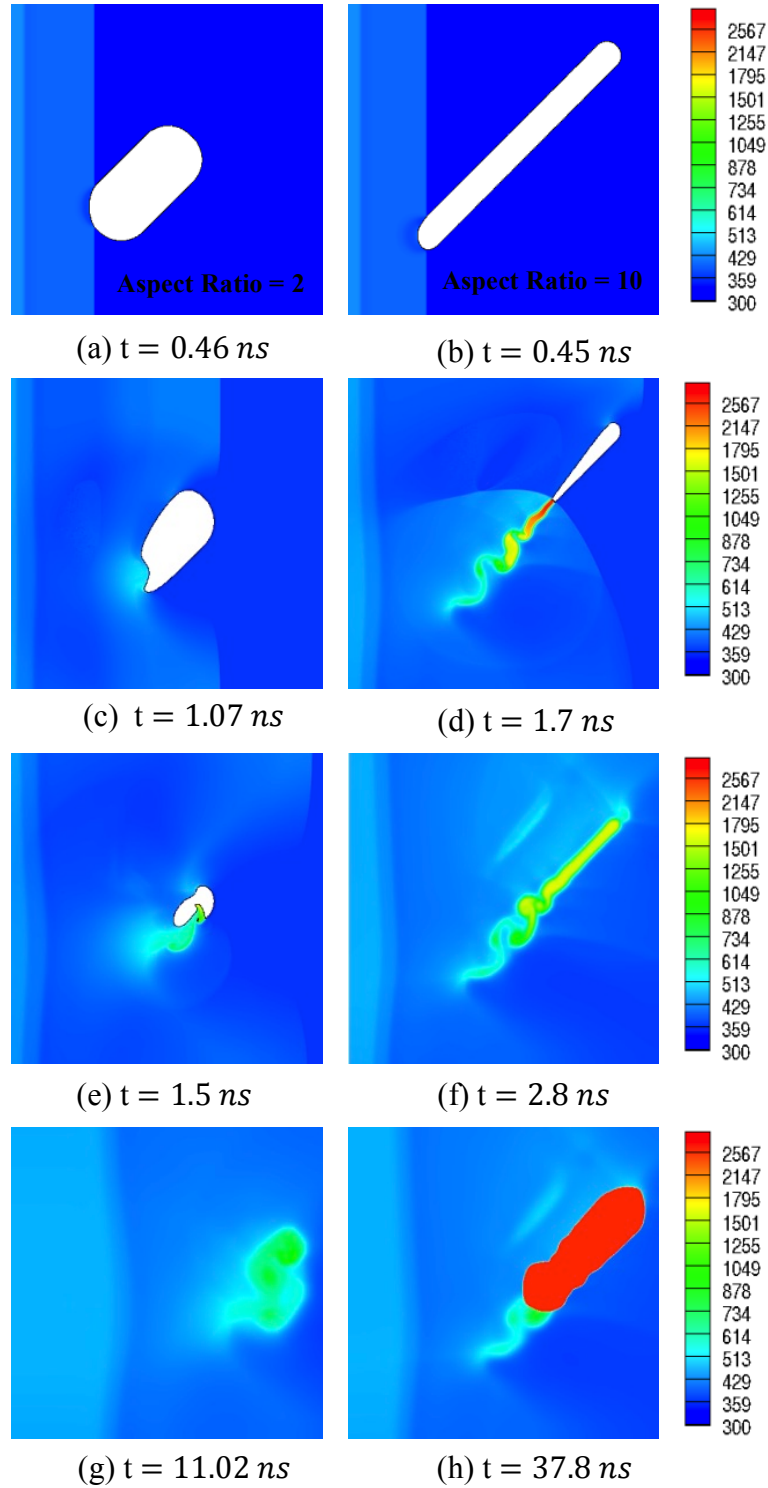


Figure 10: Temperature contour plots for the two elongated void with aspect ratio 2 and 20. The voids are oriented at an angle of  $45^\circ$  with respect to the shock wave. The computational set up is shown in Figure 2. The shock strength is  $650 \text{ m/s}$  and the pulse duration is  $0.5 \text{ ns}$ .

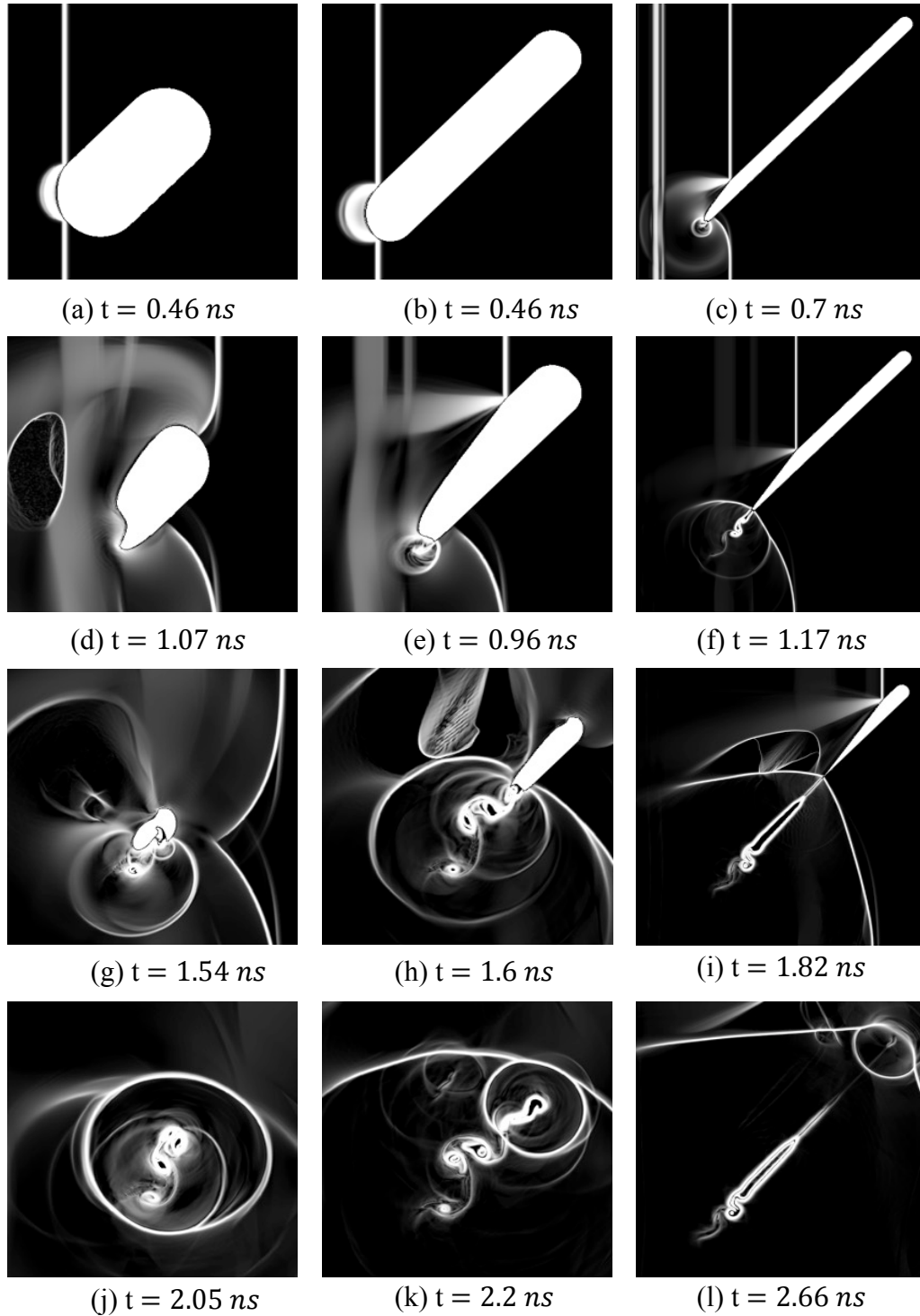


Figure 11: Numerical Schlieren plots for three elongated voids with aspect ratio 2, 5 and 20. The voids are oriented at an angle of  $45^\circ$  with respect to the shock wave. The computational set up is shown in Figure 2. The shock strength is  $650 \text{ m/s}$ .



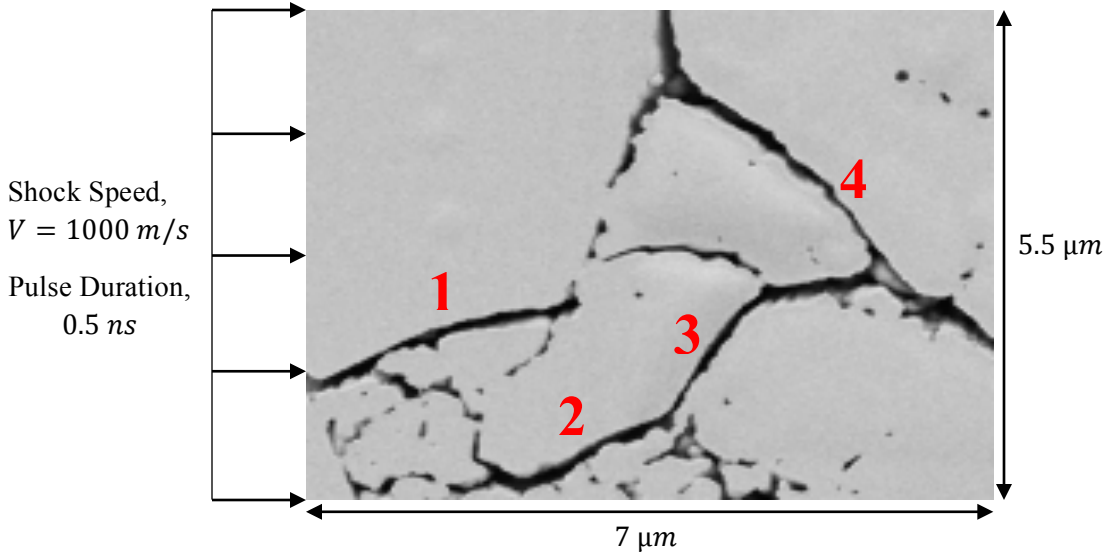
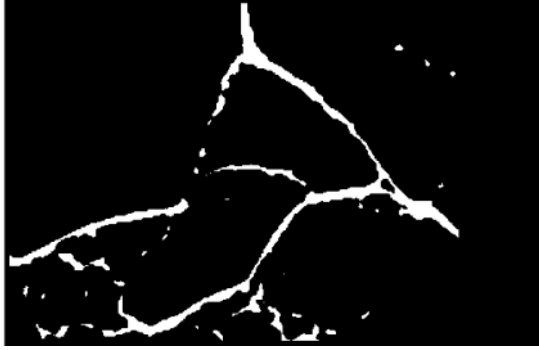
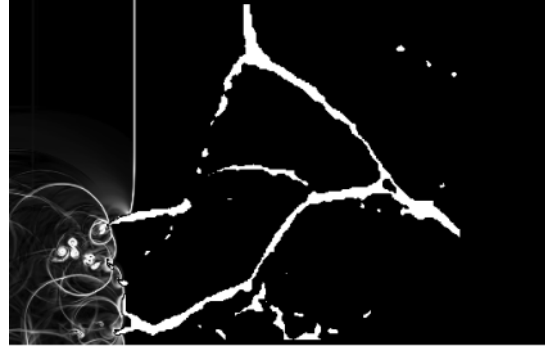


Figure 12: Numerical set up for reactive meso-scale analysis of a Class III pressed explosive sample. The sample size is  $7 \mu\text{m} \times 5.5 \mu\text{m}$ . Shock load of particle speed of  $1000 \text{ m/s}$  and pulse duration of  $0.5 \text{ ns}$  is applied from the west face of the domain boundary. There are four voids marked in the meso-structure of the sample numbered from 1 – 4 based on the orientations and aspect ratio.

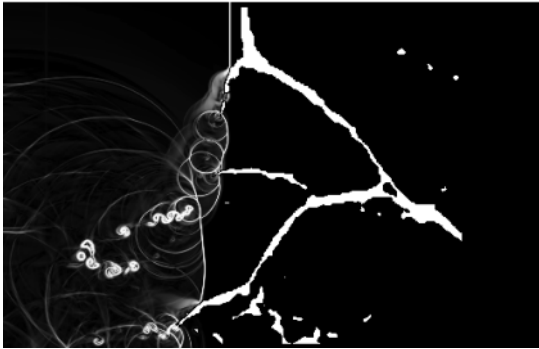




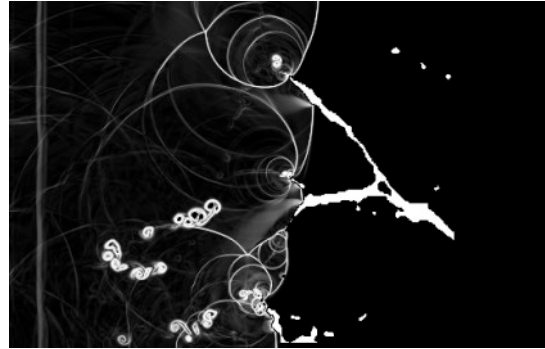
(a) Numerical Schlieren at  $t = 0.0 \text{ ns}$



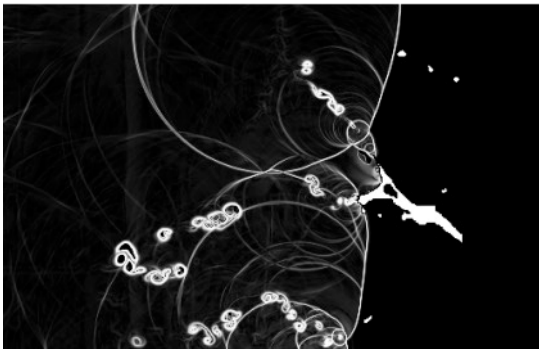
(b) Numerical Schlieren at  $t = 0.48 \text{ ns}$



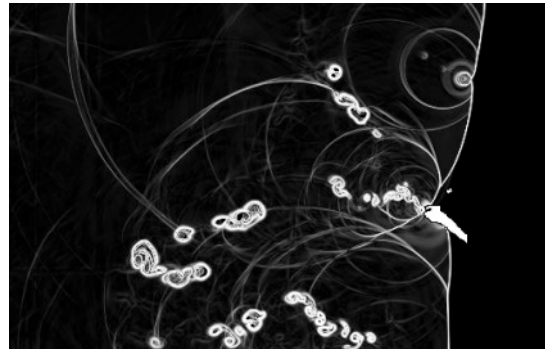
(c) Numerical Schlieren at  $t = 0.86 \text{ ns}$



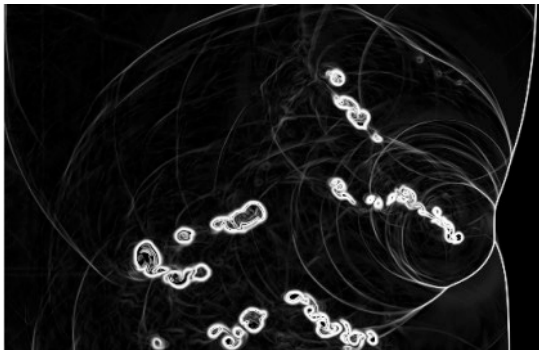
(d) Numerical Schlieren at  $t = 1.23 \text{ ns}$



(e) Numerical Schlieren at  $t = 1.55 \text{ ns}$



(f) Numerical Schlieren at  $t = 1.87 \text{ ns}$



(g) Numerical Schlieren at  $t = 2.18 \text{ ns}$

Figure 13: Numerical Schlieren plot for reactive meso-scale simulation of the Class III pressed explosive sample under the shock loading of  $1000 \text{ m/s}$  and pulse duration of  $0.5 \text{ ns}$ . Schlieren indicates the formation of the blast waves and vortices because of the subsequent collapse of the elongated voids.

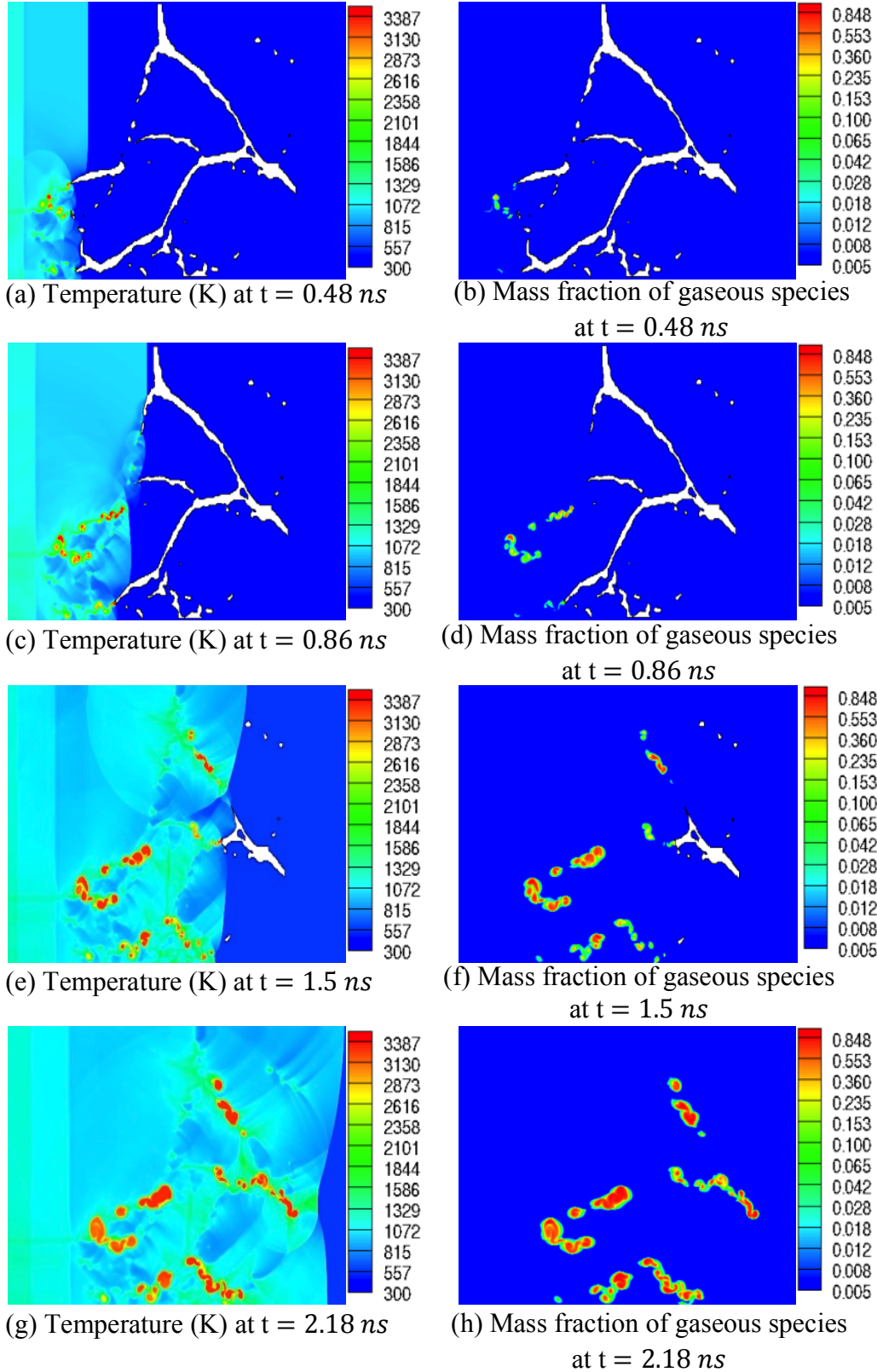


Figure 14: Temperature and the mass fraction of the final gaseous species contour plot for the reactive meso-scale simulation of the Class III pressed explosive sample under the shock loading of  $1000 \text{ m/s}$  and pulse duration of  $0.5 \text{ ns}$ . Reaction initiates at the sensitive elongated void locations with critical values of orientations and aspect ratio.